Available online at www.sciencedirect.com
SCIENCE DIRECT®
Journal of Catalysis 224 (2004) 314–325
JOURNAL OF CATALYSIS
www.elsevier.com/locate/jcat

The role of niobium in the gas- and liquid-phase oxidation on metallosilicate MCM-41-type materials

B. Kilos,[a] M. Aouine,[b] I. Nowak,[a] M. Ziolek,[a,*] and J.C. Volta [b]

[a] *A. Mickiewicz University, Faculty of Chemistry, Grunwaldzka 6, 60-780 Poznan, Poland*
[b] *Institut de Recherches sur la Catalyse, CNRS, 2 Av. Albert Einstein, 69626, Villeurbanne cédex, France*

Received 21 January 2004; revised 2 March 2004; accepted 4 March 2004

Available online 17 April 2004

Abstract

MCM-41 mesoporous molecular sieves containing Nb, V, and Mo separately and together have been synthesised and characterised by high-resolution transmission microscopy (HRTEM with EDX), N_2 adsorption isotherms, and X-ray diffraction (XRD), and tested in the oxidative dehydrogenation (ODH) of propane in the gas phase and in the liquid-phase oxidation of cyclohexene with hydrogen peroxide. For the first time, it has been documented that the incorporation of niobium during the synthesis of MCM-41 materials results in the formation of defects, the presence of which influences the selectivity in both reactions, ODH of propane to propene and epoxidation of cyclohexene. It is proposed that defect holes, generated by niobium, are convenient for access of reagents to the active species and for making the diffusion easier (particularly important in the liquid-phase reactions). NbO^- species plays the role of an electronic promoter in multimetallosilicates NbV- and NbVMoMCM-41, where vanadium is an active species. In the absence of vanadium, niobium species are active in both oxidation processes. The role of acidity in the catalysts used for both oxidation processes is considered.

Keywords: Nb; V; Mo-MCM-41; ODH of propane; Epoxidation of cyclohexene; Role of defects in catalysts

1. Introduction

Due to their abundance, the catalytic oxidative dehydrogenation of paraffins to olefins is a challenge since it is a promising route for the industrial production of chemicals. Literature data suggest that V, Nb, and Mo should be attractive for such a reaction as it was demonstrated with the Thorsteinson formulation for mild oxidation of ethane to acetic acid [1]. While the role of vanadium and molybdenum was clearly evidenced to activate the alkane (vanadium) and to play both a redox and an acidobasic role on vanadium (molybdenum), the role of niobium was not clear. It appeared that a certain isolation of the active sites was necessary to find new catalysts for mild oxidation of light alkanes as observed in previous studies [2,3]. Recently, some of us discovered that doping a VPO catalyst with niobium (Nb/V = 0.01) induced defects at the periphery of $(VO)_2P_2O_7$ crystals while Nb was simultaneously concentrating at the periphery. This fact was associated with an increase of the *n*-butane conversion for mild oxidation to maleic anhydride [4]. On the other hand, NbMCM-41 materials appeared to be active in both ODH (oxidative dehydrogenation) of propane [5] and in the liquid-phase oxidation of cyclohexene [6]. The question arises whether the incorporation of three transition metal elements (TME) V, Mo, and Nb, in a special local atomic arrangement, increases the activity and selectivity of MCM-41 materials in the oxidation reactions and what the role of niobium species is. The answer to these questions is a goal of this study.

One must to remember that various features of the catalyst are responsible for the activity and selectivity in oxidation processes performed in gas and liquid-phases. Some of them are common for both types of reactions. Grasselli [7] pointed out seven principles underpinning selective heterogeneous catalysis in the gas phase, comprising lattice oxygen, metal–oxygen bond strength, host structure, redox, multifunctionality of active sites, site isolation, and phase cooperation. Additionally, Grzybowska-Świerkosz [8] considered the role of acid-base properties of the catalyst controlling kinetics and energetics of the sorption–desorption of

* Corresponding author.
E-mail addresses: ziolek@amu.edu.pl (M. Ziolek), volta@catalyse.cnrs.fr (J.C. Volta).

0021-9517/$ – see front matter
doi:10.1016/j.jcat.2004.03.002

the reaction products. Generally for ODH of alkanes, basic catalysts seems to be more effective in the olefin formation. One should be cautious in a generalisation of this approach. It is possible to recall the systems which are quite selective in the olefin formation by ODH, like Co or Ni molybdates and which exhibit acidic centres of considerable strength. One can find in the literature [9] a correlation between the acid centres and catalytic activity in propane ODH. However, the correlation of this type cannot constitute a proof for the direct participation of acid centres in the activation of hydrocarbons. It reflects only the fact that it is the transition metal cation (Mo) which is involved in an active site for both the oxidation and the sorption of bases.

In the case of liquid-phase oxidation, some other behaviours of the heterogeneous catalysts must be considered like diffusion limitation, hydrophobicity of the catalysts, role of solvent, leaching of active species to the solution, and reducibility of metal species [10].

This paper deals with the consideration of some catalyst features, important in partially oxidation processes, both in gas (ODH of propane to propene) and liquid (epoxidation of cyclohexene) phases. Mesoporous MCM-41 material discovered in 1992 [11] was chosen as a host for multifunctional active sites located in it. These sites were generated by the incorporation of three transition metal elements (niobium, vanadium, and molybdenum together and separately) besides silicon during the synthesis. The role of defects in the obtained materials, their relation to the hysteresis loops in the nitrogen adsorption isotherms and to the activity and selectivity in both processes studied, as well as the effect of catalyst acidity are taken into consideration in this study.

2. Experimental methods

2.1. Catalyst preparation

Vanadium, niobium, and molybdenum were incorporated into the mesoporous molecular sieves of MCM-41 type during hydrothermal synthesis (373 K, 48 h). Sodium silicate (27 wt% SiO_2 in 14 wt% NaOH; Aldrich) and niobium(V) oxalate (CBMM, Brazil) were used as a silicon and niobium source, respectively, and *n*-hexadecyltrimethylammonium chloride (25 wt%; Aldrich) was applied as a surfactant. For the preparation of catalysts containing vanadium and molybdenum, vanadyl(IV) sulfate (BDH) and ammonium heptamolybdate(VI) (POCH, Poland) were sources of V and Mo, respectively. The composition of the reactant mixture depended on the assumed Si/T ratio (where T = Nb, V, Mo) which was planned as 16, or/and 32, or/and 64, or/and 128, or/and 256. In case of bi- and trifunctional systems, the following sequence of the admission of metal sources was used: niobium oxalate, vanadyl sulfate, and ammonium molybdate. The gels formed from these components were loaded into a stoppered PP (polypropylene) bottles and heated at 373 K for 24 h. The mixtures were then cooled to room temperature. The pH level was adjusted to 11 by dropwise addition of diluted sulfuric (for Mo and V) or oxalic (for Nb or Nb + V and/or + Mo) acids with vigorous stirring. These reaction mixtures were heated again to 373 K for 24 h. The resulting precipitated products were washed with distilled water and dried in air at ambient temperature. The template in the catalysts was removed by calcination at 823 K, 1 h in helium flow and 12 h in air under static conditions.

2.2. Characterisation techniques

2.2.1. X-ray diffraction (XRD)

X-ray diffraction patterns were recorded between 1 and 40° (2θ) on a Philips PW 1710 diffractometer (Cu-K_α radiation; $\lambda = 0.154$ nm) with a step size 0.02°.

2.2.2. N_2 adsorption/desorption

The surface areas and pore volumes of the TMCM-41 materials were measured by nitrogen adsorption at 77.4 K using the conventional technique on a Micromeritics 2010 apparatus. Prior to the adsorption measurements, the samples were degassed in vacuum at 573 K for 2 h. The pore diameter was determined from the adsorption branch of isotherms using a corrected algorithm (KJS-BJH) based on the Barret–Joyner–Halenda (BJH) procedure.

2.2.3. Chemical analysis

The metal contents (Nb, V, Mo) in the calcined TMCM-41 samples were determined by inductively coupled plasma emission spectroscopy (ICP) (AES-Flammes Perkin-Elmer M 1100) after solubilisation of the samples in H_2SO_4:HNO_3:HCl solutions.

2.2.4. High-resolution transmission electron microscopy (HRTEM)

HRTEM was performed with a 200-kV Jeol JEM 2010 microscope, with a point to point resolution of 0.19 nm (coefficient of spherical aberration $C_s = 0.5$ mm), and equipped with an EDS X-ray analyser Link-Isis. Samples are included in an EPON resin. Very thin slices (20–40 nm) are obtained by ultramicrotomy of the samples. The Ultramicrotome is a Leica Ultra Cut UCT equipped with a diamond knife. The slices are then recovered on a microscopy copper grid (3.05 mm; 200 mesh) previously coated with a holey-carbon film.

2.2.5. FTIR acidity measurements

Infrared spectra were recorded with a Brucker Vector 22 FTIR spectrometer (DTGS detector). Pyridine and lutidine were used as basic probes. The samples were pressed under low pressure, into a thin wafer $\sim$ 10–15 mg cm^{-2} and placed in the vacuum cell. The activation was performed first in a flow of O_2 at 723 K for 1 h. Next, the cell was cooled to RT for evacuation of oxygen. After that, the sample was outgased at 673 K for 12 h. Pyridine and lutidine were adsorbed at 373 K. The desorption was carried out for 30 min

at each of the following temperatures: 373, 423, 473, 523, and 573 K. All spectra were recorded at room temperature. The spectra shown in this paper are recalculated for the same weight of the samples—1 mg.

2.3. Catalytic tests

2.3.1. Propane oxidation

The partial oxidation reactions were carried out using a conventional fixed-bed flow reactor (diameter 16 mm) working at atmospheric pressure. The amount of 1 cm^3 of the catalyst was loaded into a U-type reactor made of quartz tube and treated in a flow of N_2 (40 $cm^3\,min^{-1}$) at 773 K for 4 h before the reaction. The reactor was equipped with a coaxial thermocouple for catalytic bed temperature profiling. The feed consisted of a mixture of propane/oxygen/nitrogen with a molar ratio 7/13/80 and a total gas flow of 17.5 $cm^3\,min^{-1}$. Catalytic experiments were carried out in the 753–823 K temperature range. Under these conditions, both external and internal diffusion limitations were absent as evidenced from the results shown in Fig. 1. Analysis of reactants and products was performed by on-line gas chromatography coupled to the outlet. Light hydrocarbons, oxygenated compounds and acids were analysed by Shimadzu GC-14B gas chromatograph—temperature programmed—with two FID detectors equipped with three columns: Durapak (for hydrocarbons separation), Carbowax 20M and AT 1200 (for oxygenate separation—aldehydes, ketones, and acids, respectively). The Durapak (*n*-octane on Porasil C; 80–100 mesh, 4 m; 1/8-inch diameter) and Carbowax (20 wt% on Chromosorb P-AW-DMCS; 60–80 mesh, 4 m; 1/8-inch diameter) columns were settled in parallel and were working at 363 K on the first FID detector. The originality of the settling was to adapt the gas analysis with the intercalation of the peaks of the different products. The AT 1200 column working at 393 K was connected to the second FID detector. A Delsi GC 121MB chromatograph with TCD detector was used in order to separate O_2, N_2, and CO at 353 K on a Tamis 5A (60–80 mesh, 2 m; 1/4-inch diameter) and CO_2 and H_2O at 353 K on a Porapak Q (80–100 mesh, 2 m; 1/4-inch diameter) column. Carbon balance was kept within 5% or below.

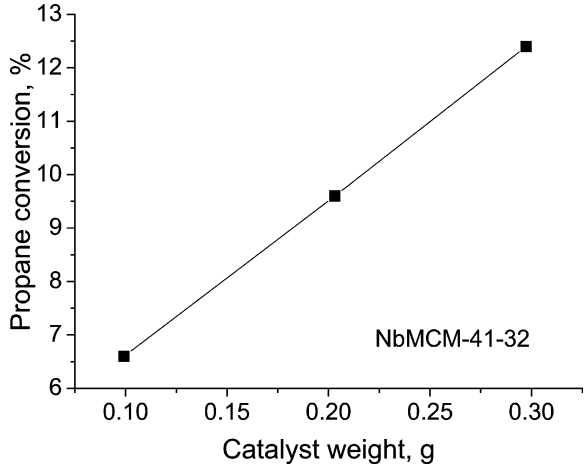

Fig. 1. Control about diffusion limitation.

2.3.2. Cyclohexene oxidation with H_2O_2

All prepared materials were tested in the oxidation of cyclohexene with hydrogen peroxide. The reaction was performed at 318 K in the liquid-phase using acetonitrile as a solvent. The catalytic reaction between cyclohexene and hydrogen peroxide was carried out in a glass flask equipped with a magnetic stirrer, a thermocouple, a reflux condenser, and a membrane for sampling. The amount of 0.04 g of a calcined catalyst was placed into the flask where the solvent was added. The oxidation was conducted simply by efficient stirring of a mixture of a solvent and a catalyst at 318 K. After stirring for 15 min, cyclohexene (2 mmol) was added, followed by the dropwise addition (10 s) of $\sim$ 34% hydrogen peroxide (2 mmol). The first analysis was done after 30 min from the beginning of the reaction. Samples were taken at regular time intervals and analysed by a gas chromatograph GC 8000 Top equipped with a capillary column of DB-1, operated with a heating program: 333 K for 15 min, ramp 10 K min^{-1} to 353 K (kept for 13 min), attached to a FID.

For both reactions, conversion of reactants and selectivity to products were calculated based on molar values, using the responses factors for all products of the reactions.

3. Results

3.1. Characterisation of the catalysts

3.1.1. Chemical analysis

Table 1 exhibits the composition of the materials used based on ICP analysis. The data clearly show that the amount of metals in the final material differs from that in the gel. It has been indicated in our previous works [12,13] that the cation size and oxidation state of metal cation do not determine the facility for transition metal inclusion into the mesoporous structure of MCM-41 type during the synthesis in a simple way. Under the synthesis conditions applied in this work, the use of the same atomic amount of metals in Nb, V, and Mo sources for preparing one transition metal containing MCM-41 lead to the following order for metal incorporation efficiency: Nb > V $\gg$ Mo. If two (Nb, V) or three (Nb, V, Mo) metals are introduced together during the synthesis, the V content is enhanced in comparison to one metal-containing samples. Niobium seems to be responsible for this feature. If V is introduced together with Nb, more vanadium is incorporated into the final mesoporous material than if only V together with Si source is used. The introduction of Mo into the framework together with Si is extremely difficult (Si/Mo ratios > 2000) under the conditions applied in this work. The use of a higher amount of Mo source leads to a higher content of Mo, but no more than $\sim$ 0.01 part of Mo used in the reagent mixture is located in the final material.

Table 1
The chemical composition of the samples (obtained from ICP analysis)

Catalyst[a]	Assumed atomic ratios	Atomic ratios					
		Si/Nb	Si/V	Si/Mo	V/Nb	Mo/Nb	Mo/V
NbMCM-41-32	Si/Nb = 32	26	–	–	–	–	–
NbMCM-41-64	Si/Nb = 64	45	–	–	–	–	–
NbMCM-41-128	Si/Nb = 128	129	–	–	–	–	–
VMCM-41-32	Si/V = 32	–	259	–	–	–	–
VMCM-41-128	Si/V = 128	–	1950	–	–	–	–
MoMCM-41-32	Si/Mo = 32	–	–	> 2000	–	–	–
MoMCM-41-128	Si/Mo = 128	–	–	> 2000	–	–	–
NbVMCM-41-51	Si/Nb = 256 Si/V = 64 V/Nb = 4/1	216	272	–	0.8	–	–
NbVMCM-41-64	Si/Nb = 128 Si/V = 128	129	879	–	0.08	–	–
NbVMoMCM-41-9.8	Si/Nb = 128 Si/V = 32 Si/Mo = 16 V/Nb = 4/1 Mo/V = 2/1	134	133	1712	2	0.08	0.08
NbVMoMCM-41-19.7	Si/Nb = 256 Si/V = 64 Si/Mo = 32 V/Nb = 4/1 Mo/V = 2/1	230	255	> 2000	0.9	< 0.06	< 0.06

[a] The last number in the catalyst symbol denotes Si/T assumed ratio; T = ∑ of transition metal atoms.

It is worthy of note that in the case of a low Si/Nb ratio in the gel (NbMCM-41-32 or 64), the real Si/Nb ratio in the final material is lower than that assumed. It can suggest that not all of Nb is in the Si–O–Nb framework but part of Nb is localised in the extraframework position. As a consequence, a chemical analysis gives rise to a lower Si/Nb ratio than assumed, indicating that part of Si from the reactant mixture was not placed into the final material. A similar feature was observed for Co-MCM-41 [14]. If Si/Nb = 128 is used in the gel, the obtained material has the identical Si/Nb ratio.

3.1.2. X-ray diffraction and low-temperature nitrogen adsorption

All the materials synthesised within this work exhibit a well-ordered hexagonal mesoporous structure of MCM-41 type with one system of pores (ca. 4 nm of diameter) and a very high specific surface area (ca. 1000 $m^2\,g^{-1}$) [12]. Table 2 summarises structural/textural data of all materials basing on XRD and low-temperature nitrogen adsorption experiments. The calcined TMCM-41 materials gave well-defined hexagonal XRD patterns with a main peak at $2\theta \sim 2^\circ$ and up to three signals in the region 3–8°. The introduction of metals slightly decreases the unit cell parameter and this decrease depends on the amount of metal introduced. It is noteworthy that all niobium-containing materials exhibit the presence of extraframework crystal phases (Nb_2O_5 or $Na_2Nb_4O_{11}$)—Table 2. The orders for the amounts of crystal phases can be estimated on the base of XRD peak intensity shown in [13]. For Nb_2O_5 it is NbMCM-41-32 > NbMCM-41-64 > NbVMoMCM-41-9.8, whereas for $Na_2Nb_4O_{11}$ the following order can be determined: NbVMCM-41-64 > NbMCM-41-128 > NbVMCM-41-51 ≫ NbVMoMCM-41-19.8.

The N_2 adsorption/desorption isotherms are of type IV in the IUPAC classification (typical of MCM-41 materials), Fig. 2. The steps of capillary condensation in primary mesopores are clearly pronounced and steep. By contrast, the isotherms of the samples prepared with high concentrations of transition metal elements (Figs. 2A(a and b) and 2B(a and b)) featured prominent hysteresis loops at $p/p_0 = 0.9$–1 indicating a considerable macroporosity or intergranular porosity. It is well known that this outcome is produced by such macropores that are connected through windows of smaller size (so-called bottleneck pores). For most niobium-containing materials an additional uncommon type H4 hysteresis is observed in $p/p_0 = 0.5$–1 (Figs. 2A(a) and 2B(a and b)). On the base of the analysis of TEM micrographs, Lin et al. [16] assigned this hysteresis loop, at $p/p_0 = 0.5$–1.0, to structural defect holes amid the nanochannels. The TEM images shown below confirmed this assignment also for Nb-containing MCM-41 samples studied in this work.

3.1.3. High-resolution transmission electron microscopy

Fig. 3 shows the micrographs of the chosen catalysts. A zoom of the hexagonal channels of MCM-41 is given. MCM-41 (Fig. 3a) shows hexagonal channels with a size of about 4 nm. HRTEM micrographs indicate the presence of defects dispersed in materials containing niobium. They are absent in the samples without Nb. For NbMCM-41 materials, the amount of defects decreases with the decrease of niobium loading (from Si/Nb = 26 to Si/Nb = 129 in the final material). The structural defects are observed in areas

Table 2
Textural/structural parameters from low-temperature N_2 adsorption/desorption and XRD results

Catalyst	Surface area (BET) ($m^2\ g^{-1}$)	Pore diameter (BJH-KJS)[b] (nm)	Wall thickness[a] (KJS)[b] (nm)	Unit cell (a_0) (nm)	Extraframework phase
MCM-41	1090	4.02	0.87	4.57	–
NbMCM-41-32	960	3.66	0.99	4.29	Nb_2O_5
NbMCM-41-64	1040	3.64	1.02	4.34	Nb_2O_5
NbMCM-41-128	930	3.65	1.04	4.33	$Na_2Nb_4O_{11}$
VMCM-41-32	1070	3.94	0.85	4.38	–
VMCM-41-128	1090	3.98	0.84	4.47	–
MoMCM-41-32	1040	3.94	0.94	4.55	–
MoMCM-41-128	1100	4.10	0.82	4.39	–
NbVMCM-41-51	970	3.62	1.00	4.51	$Na_2Nb_4O_{11}$
NbVMCM-41-64	970	3.96	0.98	4.31	$Na_2Nb_4O_{11}$
NbVMoMCM-41-9.8	1020	3.95	0.94	4.36	Nb_2O_5
NbVMoMCM-41-19.7	1020	3.97	0.90	4.46	Traces $Na_2Nb_4O_{11}$

[a] $a_0 = 2d_{100}(1/\sqrt{3})$; $w = (8/(\pi\sqrt{3}))d_{100}\sqrt{(\rho V)/(1+\rho V)}$; $t = a_0 - w/1.05$; a_0 = unit cell, w-pore diameter, t-wall thickness.
[b] BJH method modified by Kruk, Jaroniec, and Sayari (KJS) [15].

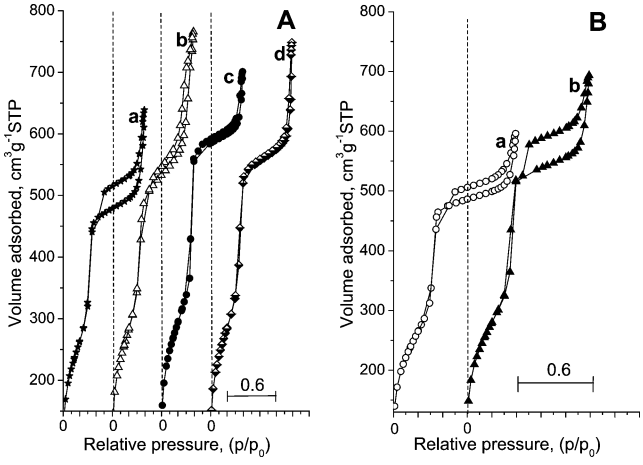

Fig. 2. Low temperature nitrogen adsorption/desorption isotherms: (A) (a) NbMCM-41-32; (b) NbMCM-41-64; (c) VMCM-41-32; (d) MoMCM-41-32; (B) (a) NbVMCM-41-51; (b) NbVMoMCM-41-9.8.

where Nb is detected by EDX. EDX investigations show that niobium species are not dispersed homogeneously. One can suggest that a kind of niobium nests is formed on the surface of niobium-containing MCM-41 materials. The concentration of Nb as well as the size of defect holes should determine a level of isolation of niobium species. There is no doubt that after dehydroxylation of the sample NbO^- and Nb^+ species are formed. They were identified in our earlier papers [17–19]. One can relate them to the SiO^- species associated with the defects observed by Dzwigaj et al. [20] in V-MCM-41 samples. Nb^+ species play the role of Lewis acid centres whereas NbO^- should be active in the electron transfer, important in partial oxidation processes (e.g., [21]). It is possible that in case of rather low niobium loading, a kind of isolation of Nb–hydroxyl pairs should be achieved (in the hydroxylated material) in the defect holes (or in their surrounding).

HRTEM micrograph (Fig. 3c) of VMCM-41-32 shows the presence of vanadium species located into the channels without modification of the size (3.8 nm). Dispersed vanadium species are also shown in HRTEM of NbVMoMCM-41-9.8 besides large defect holes containing niobium species.

3.1.4. Acidity measurements

In order to evaluate the amount and type of acidic sites, infrared spectroscopy (FTIR) of adsorbed bases has been applied. Pyridine ($pK_b = 8.8$) interacts with Lewis acid sites (LAS) giving rise to characteristic IR bands at ~ 1610 (υ_{8a} mode) and $\sim 1445\ cm^{-1}$ (υ_{19b} mode). The intensity of the υ_{19b} band is related to the number of LAS taking into account that $\varepsilon_{1450} \approx 1.5\ \mu mol^{-1}$ [22].

The FTIR study of pyridine adsorbed at 373 K followed by 30 min desorption at the same temperature allows us to estimate the Lewis acidity of the catalysts. The presence of IR bands at ~ 1610 (υ_{8a} mode) and $\sim 1445\ cm^{-1}$ (υ_{19b} mode) characterises Lewis acid centres. Fig. 4 compares chemisorption of pyridine on NbMCM-41 samples with various niobium contents. The stability of chemisorbed pyridine can be referred to the strength of Lewis acid sites and can be estimated on the basis of FTIR spectra after evacuation at various temperatures. It is clearly evidenced that the higher the niobium content, the higher the strength of Lewis acid sites. Consideration of the materials (containing mono- and multimetals) exhibiting almost the same niobium content (Table 1) allows us to propose the following order of Lewis acid strength estimated on the basis of chemisorbed pyridine shown in Fig. 5: NbVMoMCM-41-9.8 $\gg$ NbVMCM-41-64 > NbMCM-41-128.

FTIR spectra (Fig. 5) exhibit the bands due to pyridine coordinatively bounded to residual Lewis acid sites after outgasing at 423 K. The intensity of these bands diminishes in the sequence shown above. It is clear that the presence of Mo and/or V (to a lower extent) besides niobium increases the acidity. Taking into account that Lewis acidity on MoMCM-41 and VMCM-41 is negligible (very low intensity of Py-IR bands at 1610 and 1445 cm^{-1} after low-temperature, 373 K, evacuation—not shown here) one can state that vanadium

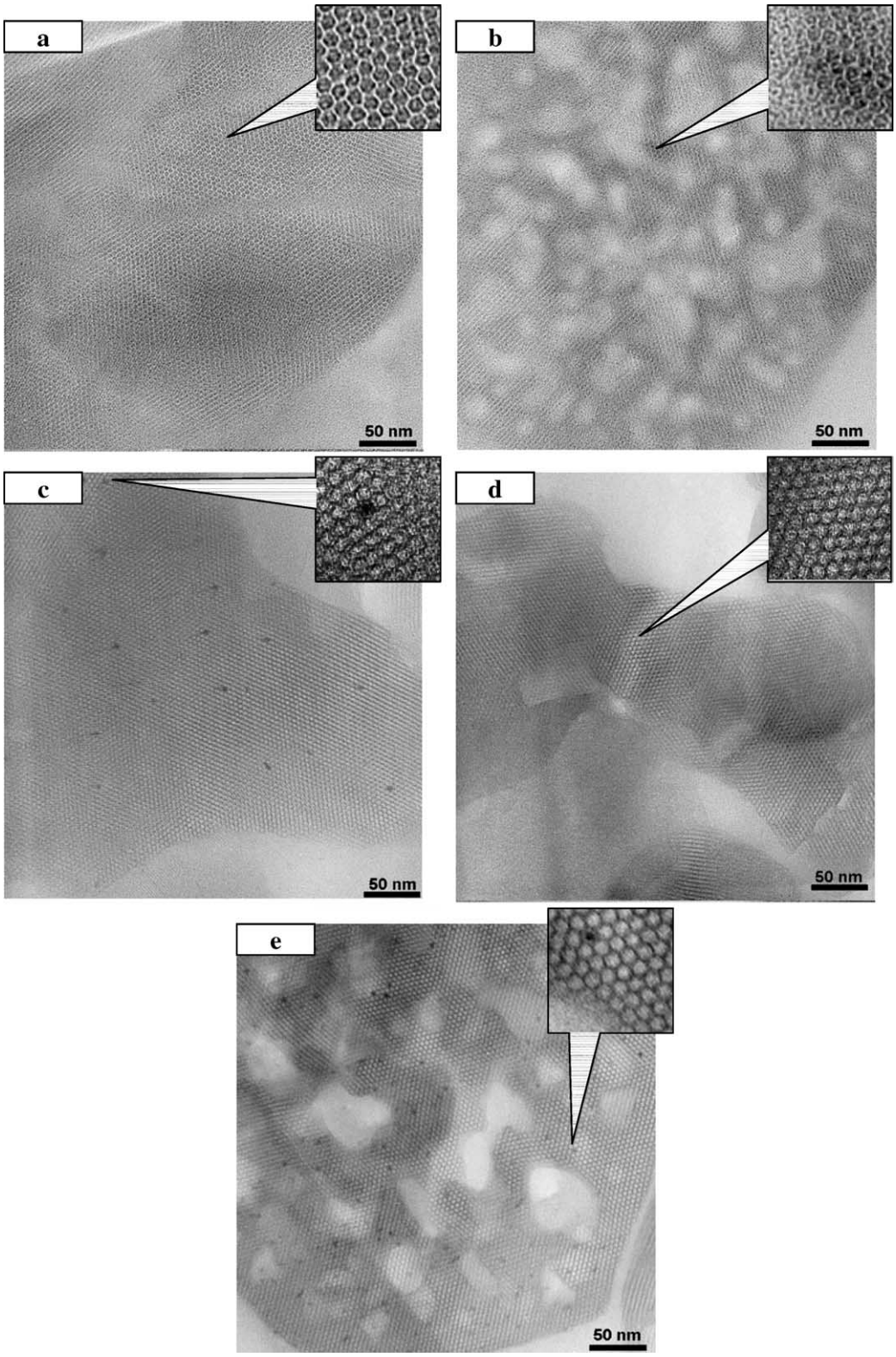

Fig. 3. HRTEM images of (a) SiMCM-41, (b) NbMCM-41-32, (c) VMCM-41-32, (d) MoMCM-41-32, (e) NbVMoMCM-41-9.8.

and molybdenum in multimetallosilicate samples promote Lewis acidity located on niobium species.

Table 3 presents the number of Lewis acid centres in the samples studied. Vanadium or molybdenum-containing samples (VMCM-41 and MoMCM-41) exhibit a low number of LAS like NbMCM-41-128. The comparison of the materials with the same number of niobium (NbVMoMCM-41-9.8; NbVMCM-41-64; NbMCM-41-128) shows the same

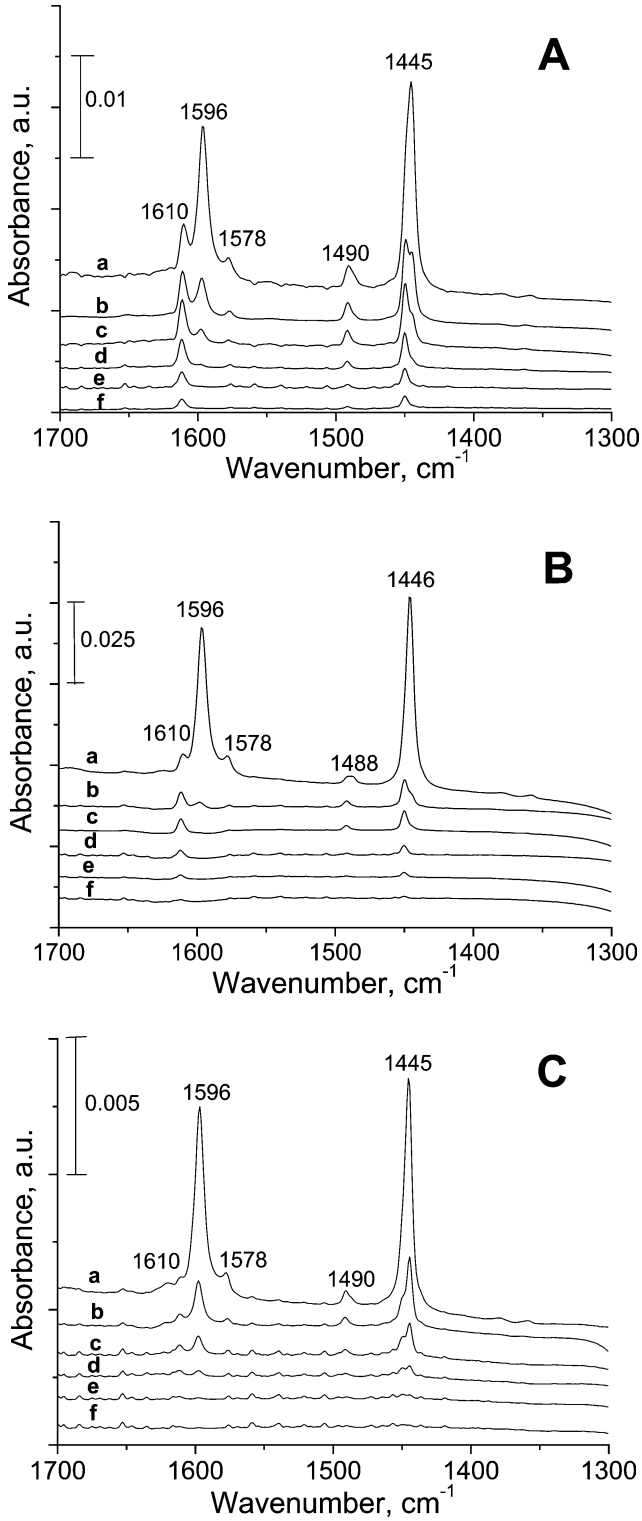

Fig. 4. FTIR spectra recalculated to 1 mg of the materials: (A) NbMCM-41-32; (B) NbMCM-42-64; (C) NbMCM-41-128 after adsorption of pyridine at 373 K (a) and desorption at 373 K (b); 423 K (c); 473 K (d); 523 K (e); 573 K (f).

sequence in the number of LAS as that presented above for the Lewis acid strength. Therefore, one can conclude that the presence of molybdenum and/or vanadium together with

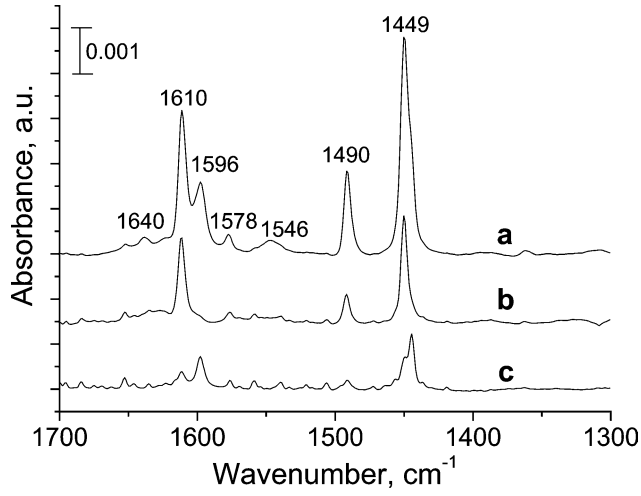

Fig. 5. FTIR spectra recalculated to 1 mg of the materials: NbVMoMCM-41-9.8 (a); NbVMCM-41-64 (b); NbMCM-41-128 (c) after pyridine desorption at 423 K.

Table 3
Number of LAS calculated per 1 g of the catalyst calculated from IR bands obtained after pyridine adsorption and desorption at 373 K ($\varepsilon_{1450} \approx 1.5$ μmol^{-1} [22])

Sample	Number of LAS × 10^{17}
NbMCM-41-32	158
NbMCM-41-64	145
NbMCM-41-128	29
VMCM-41-32	59
VMCM-41-128	23
MoMCM-41-32	20
MoMCM-41-128	18
NbVMCM-41-51	46
NbVMCM-41-64	135
NbVMoMCM-41-9.8	163
NbVMoMCM-41-19.7	83

niobium enhances also the concentration of Lewis acid centres and that these sites are located near niobium species. Most probably V and Mo make the isolation of pairs of Nb species easier which in consequence gives rise to the formation of Nb^+, NbO^- pairs upon dehydroxylation. The first one plays the role of LAS.

Pyridine interacts also with Brønsted acid sites (BAS) resulting in the appearance of a band near 1550 cm^{-1}, which is accompanied by two others near 1640–1620 cm^{-1}. Moreover, hydrogen-bound pyridine gives rise to IR bands at 1445 and 1596 cm^{-1} and weak Lewis-bound pyridine is characterised by a band at $\sim$1575 cm^{-1} [23]. Pyridine adsorption allows the estimation of Brønsted acidity only in NbVMoMCM-41-9.8 characterised by weak bands at 1640 and 1546 cm^{-1} (Fig. 5). However, for the other materials, pyridine did not detect BAS. Therefore, 2,6-dimethylpyridine (2,6-lutidine, Lu $pK_b = 7.25$), which is a stronger base than pyridine, due to a donor effect of methyl groups, has been also used in the acidity study. LuH^+ species (lutidinum) shows IR bands in the 1630–1650 cm^{-1} range characteristic of lutidine adsorbed on BAS

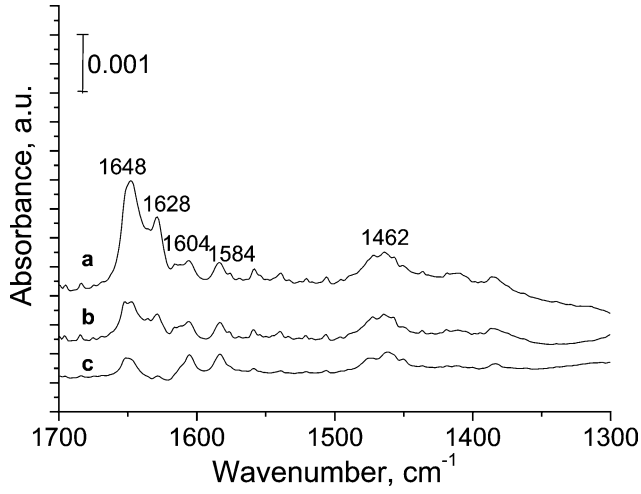

Fig. 6. FTIR spectra recalculated to 1 mg of the materials: NbVMoMCM-41-9.8 (a); NbVMoMCM-41-19.7 (b); NbVMCM-41-51 (c) after lutidine desorption at 473 K.

[24,25]. Both MoMCM-41 samples and VMCM-41-128 do not show the IR bands assigned to LuH^+. Brønsted acidity of NbMCM-41-128 is negligible. All other materials exhibit BAS with various concentrations determined by IR band intensity. Fig. 6 compares the FTIR spectra of lutidine adsorbed and desorbed at 473 K on multimetals-containing samples. The intensity of bands at 1628 and 1648 cm^{-1} on NbVMoMCM-41-9.8 with a higher metal content is higher than that on NbVMoMCM-41-19.7. Molybdenum in the neighbourhood of niobium and vanadium in MCM-41 material seems to increase the number of BAS as shown in [2] for the Mo,V/TiO_2 system. The MoMCM-41 sample presents a medium strength of Brønsted acidity (estimated on the basis of lutidine desorption temperature) among the samples studied.

3.2. Catalytic tests

3.2.1. Catalytic activity in oxidative dehydrogenation of propane

Propene, CO, and CO_2 were the main (and under conditions applied in this work—the only) reaction products formed during the oxidation of propane on the catalysts studied in this work. Since it is known that high selectivities to propene are favoured at high reaction temperatures on most often studied vanadium-containing catalysts [26–28], propane oxidation has been mainly performed in this work at the temperature range 753–823 K.

Catalytic data for propane ODH are reported in Table 4. The results are compared for approximately 6% propane conversion reached at various temperatures (758–813 K) depending on the catalysts. The stability of the reaction is obtained after ca. 1 h time on stream. It is clearly shown that the presence of niobium in the material promotes the selectivity to propene, which is the highest (above 60%) for the materials containing a low amount of niobium; i.e., niobium species are isolated. High niobium-loaded samples (NbMCM-41-32 and NbMCM-41-64) give rise to a lower propene selectivity (ca. 55 and 57%, respectively), whereas those with V or Mo but without niobium transform propane to propene at a low selectivity (ca. 29 and 36%).

For the samples with almost the same niobium content the sequence of propene selectivity is as follows: NbMCM-41-128(Si/Nb = 129) > NbVMoMCM-41-9.8(Si/Nb = 134) > NbVMCM-41-64(Si/Nb = 129). Taking into account the temperature at which ca. 6% conversion of propane is reached one can indicate the reverse sequence in the catalyst activity. It is worthy of note that among these three samples NbMCM-41-128 exhibits the lowest Lewis and Brønsted acidity.

Taking into consideration the activity at the same reaction temperature (Table 5), one can conclude that vanadium is responsible for a high propane conversion, especially as it is combined only with silicon in the MCM-41 structure (VMCM-41-32 shows the highest propane conversion). However, the total oxidation products (CO and CO_2) predominate on that catalyst. Also MoMCM-41 material shows high propane conversion. Contrary to that, the materials containing only niobium and silicon indicate the lowest propane conversion but the highest propene selectivity, especially when the Nb concentration is low.

3.2.2. Oxidation of cyclohexene

Recently, niobium-containing mesoporous molecular sieves of MCM-41 type have been recognised as very active

Table 4
Propane conversion and selectivity to propene for propane ODH (after 1 h time on stream)

Catalyst	Reaction temperature (K)	C_3H_8 conversion (%)	Selectivity (%)			C_3H_6 yield (%)
			C_3H_6	CO	CO_2	
MCM-41	758	6.1	22.8	44.1	33.1	1.2
NbMCM-41-32	813	6.6	55.1	13.2	31.7	3.6
NbMCM-41-64	821	6.6	56.7	15.3	28.0	3.7
NbMCM-41-128	819	6.6	66.3	14.9	18.8	4.4
VMCM-41-32	783	6.4	28.9	37.6	33.4	1.9
MoMCM-41-32	783	6.3	35.6	29.9	34.4	2.2
NbVMCM-41-64	803	6.1	47.8	15.7	36.4	2.9
NbVMoMCM-41-19.7	793	6.4	65.9	12.5	21.6	4.2
NbVMoMCM-41-9.8	813	6.0	60.9	13.4	25.7	3.7

Table 5
Activity for ODH of propane at 813 K (after 1 h time on stream)

Catalyst	Propane conversion (%)
NbMCM-41-32	6.6
NbMCM-41-64	4.6
NbMCM-41-128	6.0
VMCM-41-32	15.5
MoMCM-41-32	11.1
NbVMCM-41-64	9.6
NbVMoMCM-41-19.7	12.8
NbVMoMCM-41-9.8	6.0

Table 6
Results of cyclohexene oxidation at 318 K

Catalyst	Maximum conversion (%)	Selectivity (%)		
		Epoxide	Diol	Others
MCM-41	14.9	10.5	76.5	13.0
NbMCM-41-32	75.5	57.6	24.1	18.4
NbMCM-41-64	70.8	58.7	24.8	16.5
NbMCM-41-128	29.8	17.8	82.2	0
VMCM-41-32	53.8	7.7	51.6	40.7
MoMCM-41-32	10.4	5.8	89.5	4.7
NbVMCM-41-64	59.1	8.9	77.3	13.8
NbVMoMCM-41-19.7	41.2	12.0	58.8	29.2
NbVMoMCM-41-9.8	43.0	6.8	68.3	24.8
Nb/MCM-41-32	59.9	54.9	45.1	0

catalysts in the oxidation of cyclohexene [29–31]. As the reaction is usually carried out in the liquid-phase, the question arises whether it is a homogeneous or heterogeneous process; i.e., whether leaching of metal to the solution occurs. This question was answered previously by performing special experiments [6]. The reactions carried out under homogeneous conditions (by dissolving of the same amount of niobium oxalate in acetonitrile as that used for the synthesis of NbMCM-41 catalysts) proceed with a very low activity and high selectivity to cyclohexanediol. After few hours of stirring the catalyst, NbMCM-41, in the presence of hydrogen peroxide followed by the filtration of the catalysts, the reaction was carried out in the solution leached from solid after admission of cyclohexene. It shows only residual activity. There was no activity when the sample was first stirred with cyclohexene for 5 h, and after removal of the catalyst hydrogen peroxide was added to the solution. Thus one can state that niobium leaching to the solution is negligible and it does not influence significantly the activity and selectivity in the oxidation of cyclohexene in acetonitrile. Contrary to that, vanadium leaching from MCM-41 by hydrogen peroxide is very high [31]. These features must be considered in the discussion of the results presented in this work.

The results of cyclohexene oxidation with hydrogen peroxide in acetonitrile as the reaction medium performed on the catalysts applied in this work are summarised in Table 6. MoMCM-41 materials exhibit the lowest activity. However, it is necessary to point out that the content of molybdenum in these materials is very low. Most of the other samples show a high conversion of cyclohexene, but various selectivities were obtained depending on the catalyst. Of course, the selectivity is determined to some extent by the conversion level. For the indication that it is not the only reason for the difference in the selectivity, the results obtained on niobium-impregnated material (Nb/MCM-41) are also shown. The cyclohexene conversion on this sample (59.9%) is almost the same as that on NbVMCM-41 (59.1%), but the selectivity to cyclohexanediol dominates on the latter material, whereas on that containing only niobium species, the selectivity to epoxide is high. The observed difference is caused by vanadium leaching to the solution and the performance of the reaction in the homogeneous liquid-phase. In the homogeneous system, the main reaction product is cyclohexanediol formed according to the second reaction pathway shown in Fig. 7. The intermediate for its formation is epoxide. However, in the liquid-phase homogeneous system, it is not stabilised enough and is easily transformed to cyclohexanediol. Epoxide is stabilised on Lewis acid centres, which were detected on NbMCM-41 samples rich in niobium and having a large number of defects. It is also strongly held on, e.g., NbVMoMCM-41-9.8, presenting the strongest Lewis and also Brønsted acidity and a large number of defects. Moreover, too strong Brønsted acidity of the latter material causes the epoxide ring opening to become easier, increasing cyclohexanediol selectivity [10].

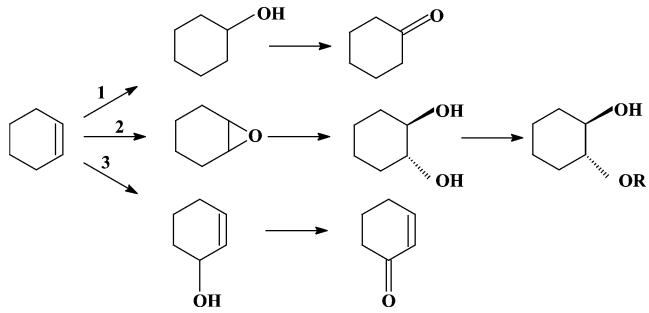

Fig. 7. Scheme of the oxidation of cyclohexene with hydrogen peroxide.

Among NbMCM-41 samples both NbMCM-41-32 and NbMCM-41-64 indicate a high cyclohexene conversion (higher for the first one) and the highest epoxide selectivity. Fig. 8 shows that the selectivity to epoxide decreases with the reaction time, most probably due to the modification of the catalyst surface by water formed from hydrogen peroxide. It has been shown earlier [6] that the admission of water to the reaction medium causes the blockade of Lewis acid sites and forms Brønsted acid sites which make the epoxide ring opening and its transformation to cyclohexanediol. Higher initial activity on NbMCM-41 materials than that on VMCM-41 one causes a higher consumption of hydrogen peroxide at the beginning of the reaction and results in the lowering of H_2O_2 concentration, which inhibits the further interaction of H_2O_2 with epoxide.

In the liquid-phase oxidation, the diffusion limitation is a very important feature if the heterogeneous catalysts are applied [19]. The defect holes especially visible in NbMCM-41-32 and NbMCM-41-64 and not observed in VMCM-41-

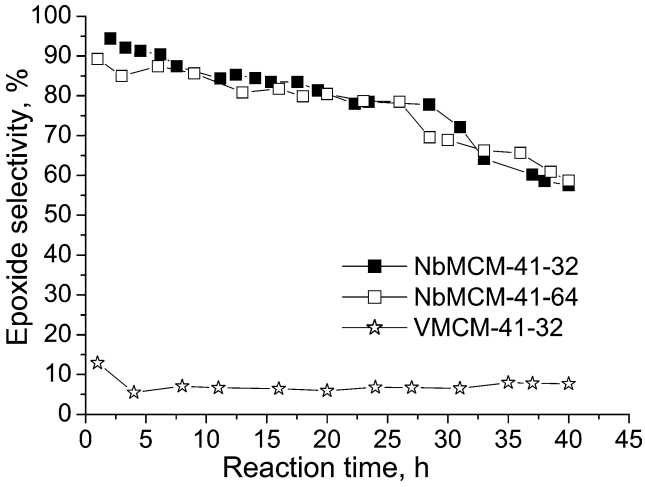

Fig. 8. Epoxide selectivity reached in the reaction of cyclohexene with hydrogen peroxide on MCM-41 materials.

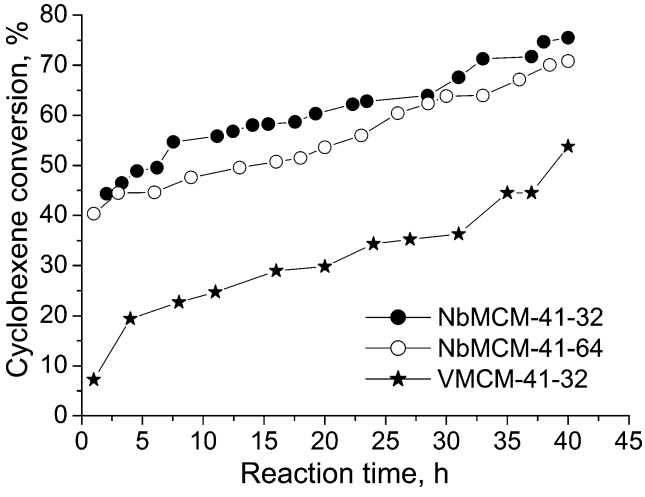

Fig. 9. Activity of the catalysts in the oxidation of cyclohexene with hydrogen peroxide.

32 seem to play a crucial role in the initial activity of the materials. Fig. 9 shows the high initial activity of the samples in which defects induce the accessibility of the active species (both Nb-containing samples), and indicates much lower activity of VMCM-41-32. The difference between cyclohexene conversion for both kinds of samples (with and without niobium) decreases with the reaction time due to vanadium leaching to the solution and the performance of the reaction in the homogeneous system.

4. Discussion

The results presented in this paper let one consider various functions of niobium located in MCM-41 structures separately and together with the other transition metals (V and/or Mo) in partial oxidation processes. Niobium plays the role of structural promoter, creating a large amount of defect cavities in the channel system observed in HRTEM images (Fig. 3) and thanks to that better interchannel connections can be achieved making the reagent transport easier. In the absence of vanadium, which is the active element in the multimetallosilicates, niobium species constitutes active centres for the activation of alkane in the gas-phase oxidation. Niobium species interacts with hydrogen peroxide in a liquid-phase alkene oxidation. Moreover, niobium species creates acidity of MCM-41 materials (Fig. 4, Table 3).

It has been documented in this paper that defect holes are dispersed in the materials containing niobium (Fig. 3). They are not present in the samples without Nb. For NbMCM-41 samples, the amount of defects decreases with diminished niobium loading. The defects are associated with the existence of a large type H4 hysteresis loop at p/p_0 between 0.5 and 1.0 (N_2 adsorption/desorption isotherms) the shape of which may be correlated with the size of defects (one can compare HRTEMs (Fig. 3) and nitrogen adsorption isotherms (Fig. 2) for NbMCM-41-32 and NbVMoMCM-41-9.8). Lin et al. [16] applying the combination of special synthesis conditions obtained similar defects in MCM-41 and AlMCM-41 materials and assigned them to the structural defect holes amid the nanochannels. Contrary to their work, the formation of a void defect structure shown in this work does not require the application of a special synthesis procedure, because the presence of a niobium source in the gel causes the defect holes in the final calcined material. These holes lead to the interconnection between linear channels. The latter causes a better interchannel diffusion, important in catalysis. It is worthy of note that structural defects are observed in areas where Nb is detected by EDX. Therefore, the defect holes make the accessibility to Nb species easier.

The comparison of the catalytic results for the ODH of propane (Table 4) with HRTEM images (Fig. 3) indicates that the selectivity to propene strongly depends on the presence of defects in the catalyst. However, there is not a simple relationship between the amount of defects in NbMCM-41 (increasing with Nb content) and the propene selectivity (decreasing with Nb content). During the dehydroxylation of NbMCM-41 materials Nb^+ (LAS) and NbO^- species are formed [18,25]. The latter may activate propane for its transformation to propene in the absence of vanadium, which is an active species, or promote electron transfer when it is present in the neighbourhood of vanadium. If Nb concentration is higher niobium dimers are formed and the selectivity turns into the total combustion products together with the increase of activity.

The activity of NbMCM-41 materials is determined also, to some extent, by the surface acidity. With the increase of Nb content the strength of Lewis acidity improves. This is evident in Fig. 4, which indicates the enhancement of the temperature necessary for pyridine desorption with the increase of Nb content. The stronger Lewis acidity causes a stronger chemisorption of propene (the ODH product) which induces the following reaction steps leading to the total combustion products. Thus, too strong acidity of the catalyst

decreases propene selectivity and enhances of the activity. Too low acidity is inconvenient of due to lowering of the activity. The combination of multimetals (Nb, V, Mo) in the MCM-41 materials allows the achievement of niobium isolation (Si/Nb = 230, in NbVMoMCM-41-19.7) and the optimum acidity generated additionally by the presence of molybdenum is obtained. It has been found earlier [2] that a small quantity of molybdenum causes a high modification of acidity. Vanadium in the materials studied seems not to be responsible for propene selectivity because V species is well dispersed in the samples (see HRTEM micrographs—Fig. 3), in agreement with the results reported in the literature (e.g., [32,33]). Meanwhile, recently [21] it has been demonstrated that the propane ODH reaction involves one-electron reduction of two V^{5+} centres to V^{4+} using one electron from each of two lattice oxygens. For that process, two V atoms are required in neighbourhood, which is not the case of the samples applied in this study. However, when isolated NbO^{-} species are located in the surrounding of V^{5+}, it promotes the electron transfer making the propene selectivity higher (one can compare the results in Table 4 for VMCM-41-32 and NbVMCM-41-64). It is worthy of note that according to our earlier study [13] only about half of niobium is located on the surface (the other inside the walls), whereas vanadium is dispersed on the surface of the material. Moreover, niobium species are agglomerated in the surrounding (or inside) defect holes, as shown in this paper. Therefore, despite a much higher total amount of niobium in comparison with that of vanadium the real V/Nb ratio on the surface is higher than that calculated from the total amount of both metals (Table 1).

There is no evidence in our study for the role of extraframework niobium phases observed by XRD (Table 2) for the propane ODH (Tables 4 and 5). One cannot find any clear relationship of activity and/or selectivity and the presence and/or nature of extraframework niobio-oxygenate crystal phases.

Contrary to the propane ODH reaction, in the oxidation of cyclohexene, the increase of Nb content causes the enhancement of selectivity to epoxide if NbMCM-41 samples are used (Table 6). Multimetallosilicate materials (NbV- and NbVMoMCM-41) exhibit very low epoxide selectivity due to leaching of vanadium to acetonitrile medium. Vanadium in homogeneous system catalyses mainly the cyclohexanediol formation.

In contrast to the gas-phase oxidation, in the liquid-phase, the diffusion effect is more important for the catalytic reaction. Therefore, in the epoxidation of cyclohexene, the activity and epoxide selectivity are related to the amount of defects proportional to the concentration of Nb. The easy access to the active niobium species located mainly in the surrounding (or inside) the defect holes seems to limit the reaction rate. It gives a relatively high initial reaction rate (Fig. 8) causing a lowering of the second reaction step leading to cyclohexanediol formation.

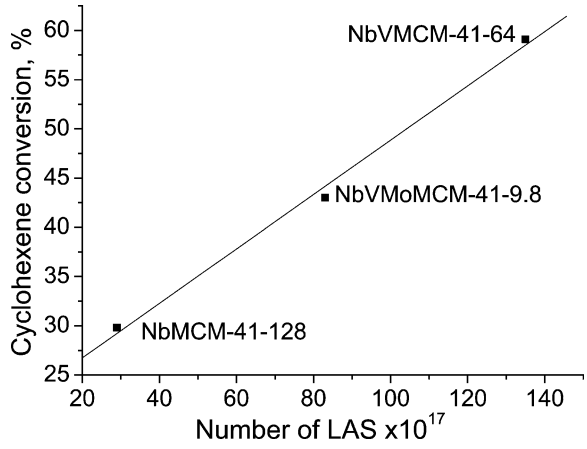

Fig. 10. Relationship between Lewis acidity and cyclohexene conversion in the reaction with hydrogen peroxide at 318 K.

The presence of Brønsted acid centres is disadvantageous for the liquid-phase oxidation of cyclohexene. It induces the epoxide chemisorption resulting in ring opening and cyclohexanediol formation. Lewis acidity enhances the cyclohexene conversion. The linear relationship between cyclohexene conversion and the number of Lewis acid sites is observed (Fig. 10) for the samples containing almost the same amount of niobium.

The results presented in this paper show a multifunctional character of niobium species located in the framework of MCM-41 materials. Studies are in progress in order to better characterise the catalysts containing various combinations of metal content in MCM-41 matrix and their local interaction. On this basis, one can expect the optimisation of the catalysts effective in both types of oxidation processes.

To conclude, one can state that niobium species in multimetallosilicate MCM-41 materials can play the role of electronic promoter, particularly important in the ODH of propane, and/or structural promoter (creates defect holes), making the access of reagents to the active species easier (mainly indicated in the liquid-phase oxidation). In the absence of vanadium, niobium species acts as the active centres in the both reactions studied. Moreover, niobium generates Lewis acidity in the catalysts.

Acknowledgments

One of us is indebted to the EC for financial support through Postfellowship Contract HMPT-CT-2000-00163. The Polish State Committee for Scientific Research (KBN—Grant 3 T09A 100 26; 2004–2006) is acknowledged for financial support. Acknowledgment is made to the CBMM (Brazil) for supplying niobium(V) oxalate.

References

[1] E.M. Thorsteinson, T.P. Wilson, F.G. Young, P.H. Kasai, J. Catal. 52 (1978) 116.
[2] M. Roy, H. Ponceblanc, J.C. Volta, Top. Catal. 11 (2000) 101.

[3] J.C. Volta, Top. Catal. 15 (2001) 121.
[4] A.M. Duarte de Farias, W.A. de Gonzalez, P.G. Pries de Oliveira, J.G. Eon, J.M. Herrmann, M. Aouine, S. Loridant, J.C. Volta, J. Catal. 208 (2002) 238.
[5] M. Ziolek, A. Lewandowska, B. Grzybowska, A. Klisinska, React. Kinet. Catal. Lett. 80 (2003) 199.
[6] I. Nowak, B. Kilos, M. Ziolek, A. Lewandowska, Catal. Today 78 (2003) 487.
[7] R.K. Grasselli, Top. Catal. 21 (2002) 79.
[8] B. Grzybowska-Świerkosz, Top. Catal. 11/12 (2000) 23.
[9] K.H. Lee, Y.S. Yoon, W. Ueda, Y. Moro-Oka, Catal. Lett. 46 (1997) 267.
[10] M. Ziolek, Catal. Today, in press.
[11] C.T. Kresge, M.E. Leonowicz, W.J. Roth, J.C. Vartuli, J.S. Beck, Nature 359 (1992) 710.
[12] M. Ziolek, I. Nowak, B. Kilos, I. Sobczak, P. Decyk, M. Trejda, J.C. Volta, J. Phys. Chem. Solids 65 (2004) 571.
[13] B. Kilos, J.-C. Volta, I. Nowak, P. Decyk, M. Ziolek, Stud. Surf. Sci. Catal., in press.
[14] W.A. Carvalho, P.B. Varaldo, M. Wallau, U. Schuchardt, Zeolites 18 (1997) 408.
[15] M. Kruk, M. Jaroniec, A. Sayari, Langmuir 13 (1997) 6267.
[16] H.-P. Lin, S.-T. Wong, Ch.-Y. Mou, Ch.-Y. Tang, J. Phys. Chem. B 104 (2000) 8967.
[17] M. Ziolek, I. Nowak, I. Sobczak, A. Lewandowska, P. Decyk, J. Kujawa, Stud. Surf. Sci. Catal. 129 (2000) 813.
[18] M. Ziolek, I. Sobczak, A. Lewandowska, I. Nowak, P. Decyk, M. Renn, B. Jankowska, Catal. Today 70 (2001) 169.
[19] M. Ziolek, Catal. Today 78 (2003) 47.
[20] S. Dzwigaj, J.-M. Krafft, M. Che, S. Lim, G.L. Haller, J. Phys. Chem. B 107 (2003) 3856.
[21] K. Chen, A.T. Bell, E. Iglesia, J. Catal. 209 (2002) 35.
[22] S. Khabtou, T. Chevreau, J.C. Lavalley, Micropor. Mater. 3 (1994) 133.
[23] B. Chakraborty, B. Viswanathan, Catal. Today 49 (1999) 253.
[24] P.A. Jacobs, C.F. Heylen, J. Catal. 34 (1974) 267.
[25] M. Ziolek, I. Nowak, J.C. Lavalley, Catal. Lett. 45 (1997) 259.
[26] T. Blasco, J.M. Lopez Nieto, Appl. Catal. A 157 (1997) 117.
[27] M. Puglisi, F. Arena, F. Frusteri, V. Sokolovski, A. Parmaliana, Catal. Lett. 41 (1996) 41.
[28] B. Solsona, T. Blasco, J.M. Lopez Nieto, M.L. Pena, F. Rey, A. Vidal-Moya, J. Catal. 203 (2001) 443.
[29] J. Xin, J. Suo, X. Zhang, Z. Zhang, New J. Chem. 24 (2000) 569.
[30] M. Ziolek, A. Lewandowska, B. Kilos, I. Nowak, in: Proc. of the 4th World Oxidation Congress, Potsdam, 16–21 September 2001, in: Book of Extended Abstracts, vol. I, 2001, p. 79.
[31] M. Ziolek, A. Lewandowska, M. Renn, I. Nowak, Stud. Surf. Sci. Catal., in press.
[32] B. Grzybowska, J. Słoczyński, R. Grabowski, K. Samson, I. Gressel, K. Wcisło, L. Gengembre, Y. Barbaux, Appl. Catal. A 230 (2002) 1.
[33] G.C. Bond, J.P. Zurita, S. Flamerz, P.J. Gellings, H. Bosch, J.G. Van Ommen, B.J. Kip, Appl. Catal. A 22 (1986) 361.